VOL. 18, NO. 11 AIAA JOURNAL NOVEMBER 1980

ARTICLE NO. 79-1513R

Progress in Finite-Volume Calculations for Wing-Fuselage Combinations

D. A. Caughey*
Cornell University, Ithaca, N.Y.
and
Antony Jameson†
New York University, New York, N.Y.

Progress in the application of finite-volume methods to the calculation of transonic potential flows past general wing-body combinations is reviewed. Two different methods of generating boundary-conforming grids are investigated, and the results compared to provide an estimate of solution sensitivity to grid geometry. Both conservative and quasiconservative difference schemes are used in one of the coordinate systems. Results show that the error introduced by the quasiconservative formulation seems to be small, although a one-dimensional analysis suggests that schemes of this type may violate conservation of mass, except in the limit when all shocks are weak. Comparison of calculated results with experimental data for realistic fuselage geometries clearly shows the importance of modeling the effect of fuselage geometry upon the wing pressure distribution.

I. Introduction

THE development of finite-difference methods for the prediction of transonic flows about realistic aircraft configurations has been much more rapid in cases for which the small-disturbance approximation is applicable than when the full potential equation must be solved. This is due in large part to the geometrical simplification afforded by use of the mean-surface approximation when satisfying the body-surface boundary conditions. This approximation is consistent with the accuracy of the small-disturbance equation, and generally allows the use of a simple Cartesian coordinate system regardless of the complexity of the body geometry. In many cases, however, the inaccuracy associated with the small-disturbance approximation and, in particular, that due to the singularity at blunt or rounded leading edges, makes the use of the full potential equation desirable.

The accurate specification of boundary conditions when using the full potential equation requires either that the calculation be perfomed in a boundary-conforming (or body-fitted) coordinate system,[1] or that interpolation formulas be applied at the body surface.[2,3] The complexity of the program logic required to determine and properly account for all the possible mesh-surface intersections, and the inefficiency of clustering mesh lines near the body surface when using a Cartesian grid make the former approach attractive.

The generation of a suitable boundary-conforming coordinate system, at least for realistic geometries, is not a trivial matter. The task is made much simpler if we require that the transformation be defined only locally. This is the primary advantage of the finite-volume techniques[4,5] and forms the basis of their relationship to finite-element methods. In this paper we take advantage of this simplification, constructing boundary-conforming coordinate systems for a class of wing-fuselage configurations using sequences of simple conformal and shearing transformations. The labor of transforming the potential equation under this sequence of mappings would be prohibitive, but the finite-volume methods require only local knowledge of the transformations; i.e., the coordinates of the corners of each mesh cell.

In the following section, both the conservative and quasiconservative formulations of the finite-volume methods will be reviewed. The construction of the two mesh systems generated for the application of the technique to wing-fuselage calculations will then be described. Finally, results will be presented which indicate the lack of sensitivity of the results to the details of mesh geometry; show that the error introduced by the quasiconservative formulation seems to be small; and show promising agreement with experimental data for practical wing-fuselage geometries.

Presented as Paper 79-1513 at the AIAA 12th Fluid and Plasma Dynamics Conference, Williamsburg, Va., July 23-25, 1979; submitted Aug. 23, 1979; revision received April 21, 1980.

Index categories: Aerodynamics; Computational Methods; Transonic Flow.

*Associate Professor, Sibley School of Mechanical and Aerospace Engineering. Member AIAA.

†Professor of Computer Science, Courant Institute of Mathematical Sciences. Member AIAA.

II. Analysis

A. Finite-Volume Schemes

The equations of steady, inviscid, isentropic flow can be represented as follows. Let x,y and z be Cartesian coordinates and u,v, and w be the corresponding components of the velocity vector q. Then the continuity equation can be written as

$$(\rho u)_x + (\rho v)_y + (\rho w)_z = 0 \tag{1}$$

where ρ is the local density. This is given by the isentropic law

$$\rho = \left[1 + \frac{\gamma - 1}{2} M_\infty^2 (1 - q^2)\right]^{\frac{1}{\gamma - 1}} \tag{2}$$

where γ is the ratio of specific heats, and M_∞ is the freestream Mach number. The pressure p and the speed of sound a follow from the relations

$$p = \rho^\gamma / (\gamma M_\infty^2) \tag{3}$$

and

$$a^2 = \rho^{\gamma - 1} / M_\infty^2 \tag{4}$$

It follows from Eqs. (2-4) that

$$\frac{d\rho}{d(q^2/2)} = -\rho / a^2 \tag{5}$$

whence Eq. (1), upon multiplication by a^2/ρ can be written

$$a^2(u_x+v_y+w_z)-(uQ_x+vQ_y+wQ_z)=0 \tag{6}$$

where $Q=q^2/2$.

Consider now a transformation to a new set of coordinates X,Y,Z. Let the Jacobian matrix of the transformation be defined by

$$H=\begin{Bmatrix} x_X & x_Y & x_Z \\ y_X & y_Y & y_Z \\ z_X & z_Y & z_Z \end{Bmatrix} \tag{7}$$

and let h denote the determinant of H. The metric tensor of the new coordinate system is given by the matrix $G=H^TH$, and the contravariant components of the velocity vector U,V,W are given by

$$\begin{Bmatrix} U \\ V \\ W \end{Bmatrix} = H^{-1}\begin{Bmatrix} u \\ v \\ w \end{Bmatrix} = G^{-1}\begin{Bmatrix} \phi_X \\ \phi_Y \\ \phi_Z \end{Bmatrix} \tag{8}$$

where ϕ is the velocity potential. Upon multiplication by h, Eq. (1) can, therefore, be written

$$(\rho hU)_X+(\rho hV)_Y+(\rho hW)_Z=0 \tag{9}$$

Equation (9) can also be expanded in a form analogous to the usual quasilinear form, and upon multiplication by a^2/ρ becomes

$$a^2((hU)_X+(hV)_Y+(hW)_Z)-(UQ_X+VQ_Y+WQ_Z)=0 \tag{10}$$

Equations (9) and (10) are the starting points for the fully conservative and quasiconservative finite-volume schemes, respectively. Equation (9) has the advantage of being in divergence form, while Eq. (10) avoids the explicit determination of the density [which, in general, requires that a fractional power be taken, according to Eq. (2)]. Both forms avoid the explicit introduction of second derivatives of the transformation.

The finite-volume schemes corresponding to Eqs. (9) and (10) are constructed by assuming separate trilinear variations of the independent and dependent variables within each mesh cell. In this way, the derivatives needed to calculate the Jacobian matrices, metric tensor, and velocity components can be expressed in terms of the values of the coordinates and velocity potential at the corners of each mesh cell. Equation (9) is represented by conserving fluxes across the boundaries of auxiliary cells whose faces are chosen to be midway between the faces of the primary mesh cells. The fluxes are determined using values of the velocities calculated at the primary cell centers. This has the advantage of requiring only one density evaluation per mesh point, but also has the undesirable effect of decoupling the solution at odd- and even-numbered points of the grid, and suitable recoupling terms must be added to stabilize the solution. Equation (10) is represented by suitable differences of the velocity components evaluated at the midpoints of the primary cell edges. The resulting equations are strongly coupled at odd and even points, but this scheme requires the evaluation of three velocities per mesh point (in three-dimensional problems). Nevertheless, the resulting scheme is only marginally less efficient than the fully conservative scheme for Eq. (9), since the density need not be evaluated.

Both schemes are stabilized in supersonic regions by the explicit addition of an artificial viscosity, chosen to emulate the directional bias introduced by the rotated-difference scheme of Jameson.[6] This artificial viscosity is added in divergence form in both schemes. Thus, the scheme corresponding to Eq. (9) is fully conservative, while that corresponding to Eq. (10) is termed quasiconservative, since the equation itself is differenced in its quasilinear or nondivergence form. Results of the two schemes appear to be in close agreement for the cases calculated to date. The quasiconservative scheme should be used with caution, however, since there is no convincing proof that it produces mass-conserving shocks. In fact, a simple, one-dimensional argument suggests that the jump conditions consistent with the quasiconservative formulation are mesh-dependent, and do not converge uniformly as the mesh is refined (see Appendix).

The difference equations resulting from either formulation are solved by successive line overrelaxation. The relaxation process is viewed as a discrete approximation to an equivalent time-dependent process, following Garabedian[7] and Jameson.[6] The insight provided by this procedure is helpful in constructing convergent and stable iterative schemes.

Further details regarding the difference approximation, artificial viscosity, and iterative schemes are contained in Refs. 4 and 5 for the conservative and quasiconservative formulations, respectively.

B. Grid Generation

The class of geometries to be analyzed is illustrated in Fig. 1. A typical example consists of a swept, tapered wing of arbitrary planform, dihedral, and section shape mounted upon a finite fuselage of varying cross-sectional area and shape. Let x,y,z be Cartesian coordinates in the streamwise, vertical, and spanwise directions, respectively; the geometry and solution are assumed to be symmetric about the plane $z=0$.

An important advantage of the finite-volume methods is their decoupling of the solution procedure from the grid-generation step. This permits the grid to be generated in any convenient manner. An attractive procedure is to generate the boundary-conforming grid using a sequence of simple, analytically defined transformations. Conformal mappings can frequently be used as building blocks in this procedure, and are attractive because of their many desirable properties (such as orthogonality). The finite-volume calculations to be described were performed on two different coordinate meshes, whose construction will be described in this section.

Cylindrical/Wind-Tunnel Grid

The first mesh system to be described is a generalization of the transformation sequence introduced in Ref. 5 to allow the fuselage to have a noncircular cross section. Let r and θ be polar coordinates in the crossflow planes, defined by

$$r=(y^2+z^2)^{1/2}, \quad \theta=\arctan(y/z) \tag{11}$$

In each cross plane, the fuselage surface is defined by $r=R_f(x,\theta)$, and a normalized radial coordinate $\bar{r}$ is defined by

$$\bar{r}=[r-R_f(x,\theta)]/[R_t-R_f(x,\theta)] \tag{12}$$

where R_t is the radius of the cylindrical surface passing through the wing tip. The wing sweep and dihedral are normalized out by referencing the coordinates in each surface of constant $\bar{r}$ to the location of a singular line $x_s(\bar{r})$, $\theta_s(\bar{r})$ passing just inside the leading edge of each wing section according to

$$\bar{x}=(x-x_s(\bar{r}))/c(\bar{r})+\log 2 \tag{13a}$$

$$\bar{\theta}=2(\theta-(1-4\theta^2/\pi^2)\theta_s(\bar{r})/[1-4\theta_s^2(\bar{r})/\pi^2]) \tag{13b}$$

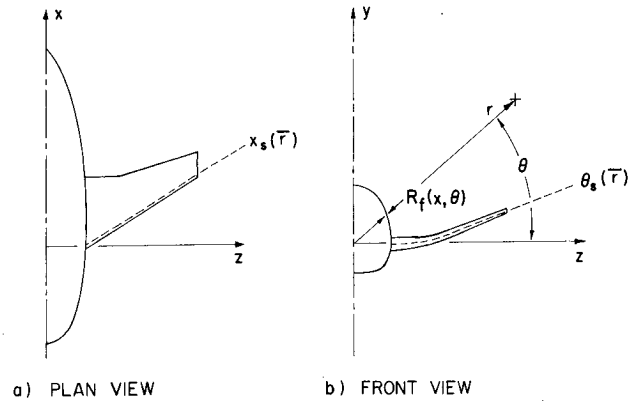

Fig. 1 Wing-fuselage geometry.

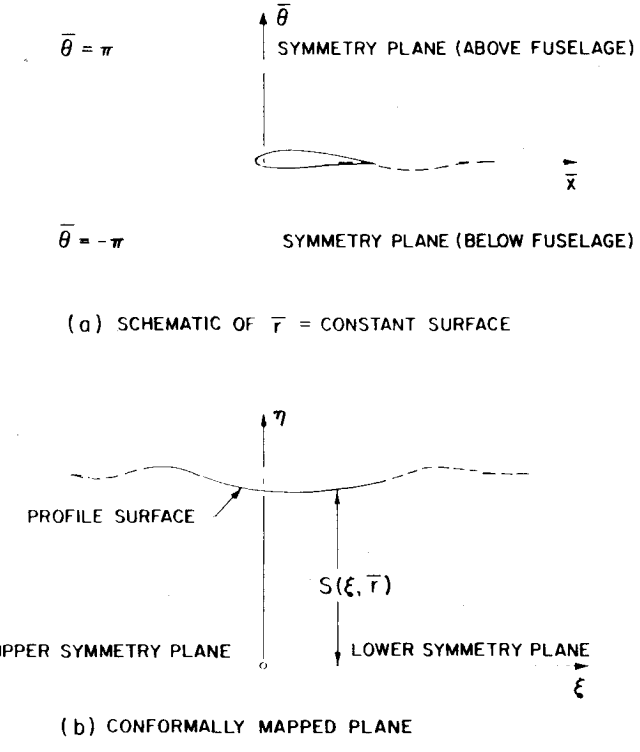

Fig. 2 Transformation sequence for wind tunnel mapping.

where $c(\bar{r})$ is the local chord length.

In a surface of constant $\bar{r}$ intersecting the wing surface (i.e., for $\bar{r} \leq 1$), the geometry looks like that in Fig. 2a. The conformal transformation[8]

$$\bar{x} + i\bar{\theta} = \log[1 - \cosh(\xi + i\eta)] \tag{14}$$

maps these surfaces to the geometry shown in Fig. 2b. The width of the strip $S(\xi,\bar{r})$ defining the wing surface is a slowly varying function if the location of the singular line has been carefully chosen. Thus the introduction of

$$X = \xi, \quad Y = \eta / S(\xi,\bar{r}), \quad Z = \bar{r} \tag{15}$$

results is a nearly orthogonal coordinate system in the planes $Z = \text{const}$.

A Cartesian grid is introduced into the X, Y, Z domain for

$$-X_{\lim} \leq X \leq X_{\lim}, \quad 0 \leq Y \leq 1, \quad 0 \leq Z \leq Z_{\lim} \tag{16}$$

where $X_{\lim}$ and $Z_{\lim}$ are chosen sufficiently large that the freestream boundary condition can be specified on these surfaces. Suitable one-dimensional stretching functions are introduced in the X, Y, and Z directions to cluster mesh surfaces in the vicinity of the body. This stretched Cartesian grid in the X, Y, Z space is then transformed back to give the Cartesian (i.e., x,y,z) coordinates of each mesh point.

The implementation of the transformation sequence described above is complicated by the two-dimensional interpolations required to define $S(\xi,\bar{r})$ as a function of the input wing geometry and $R_f(x,\theta)$ as a function of the input fuselage data. This is accomplished by a sequence of spline fits for the wing surface description, and a spline fit of the coefficients of a Fourier decomposition of the fuselage cross sections.

The fuselage cross sections are input at a number of axial stations. At each input station the cross-section data are used to determine the coefficients a_{ij} of the decomposition of R_f according to

$$R_f(x_i,\theta) = \sum_{j=1}^{m} a_{ij} \cos j(\theta + \pi/2) \tag{17}$$

Only cosine terms are necessary since the fuselage is assumed symmetric about the plane $\theta = \pm\pi/2$. For each Fourier component (i.e., each j), the coefficients a_{ij} are then considered to be continuous functions of x and are fit with splines.

The input wing geometry is then mapped to the $\bar{x},\bar{r},\bar{\theta}$ system using the interpolated values of a_{ij} to calculate R_f from Eq. (17) for each input point on the wing surface. To obtain the wing section shapes in the computational surfaces $\bar{r} = \text{const}$, a spanwise spline is fit through each set of corresponding points at the input stations, and then interpolated upon. Within each surface of $\bar{r} = \text{const}$, the conformal mapping of Eq. (14) is applied, and points corresponding to the required mesh in X, Y are determined using a spline to interpolate values of $S(\xi,\bar{r})$ in the ξ direction. The physical coordinates of the grid points are obtained by following the reverse procedure: Calculating $\bar{x}$ and $\bar{\theta}$ from Eq. (14), using Eqs. (13) to determine x and θ, Eq. (12) to determine r, and finally Eqs. (11) to give the Cartesian coordinates.

The most time-consuming step in this procedure is the calculation of $R_f(x,\theta)$ required in Eq. (12) for each mesh point. This involves interpolating on splines to find the Fourier coefficients required in Eq. (17), then summing the cosine series. The Fast Fourier Transform technique is, unfortunately, not applicable since the θ values at which the values of R_f are required are not uniformly spaced. Even so, the computation time required for the mesh generation step is a small fraction of the time required for the transonic part of the calculation. On a 122,880 cell grid, the mesh generation requires less time than that for 4 relaxation sweeps when the fuselage cross section is defined by 17 Fourier components at each of 21 axial stations.

Joukowsky/Parabolic Grid

The second grid system to be described is a generalization to allow incorporation of a fuselage to the sequence used to transform the governing equation in Refs. 6 and 9 for isolated wing calculations.

In each plane of constant x, a Joukowsky transformation is performed to reduce the fuselage cross section to a near slit using the mapping

$$\eta + i\zeta = ((y - y_0) + iz) + b^2 / ((y - y_0) + iz) \tag{18}$$

Here $y_0(x)$ is the ordinate of the mean line of the fuselage in the symmetry plane and b is the fuselage half-height (see Fig. 3a). Next, the detailed shape of the fuselage cross section is sheared out according to

$$x = x, \quad \eta = \eta, \quad Z = \frac{\zeta - Z_0(x,\eta)}{\zeta_t - Z_0(x,\eta)} \tag{19}$$

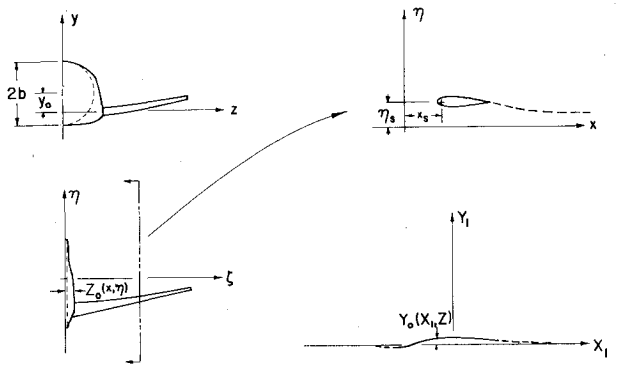

a) Joukowsky transformation b) Square root transformation

Fig. 3 Transformation sequence for Joukowsky-parabolic grid.

where ζ_t is the value of ζ at the wing tip, and $Z_0(x,\eta)$ is the height of the mapped fuselage surface above the plane $\zeta=0$. The wing surface is then unwrapped in planes of constant Z about a line $x_s(Z)$, $\eta_s(Z)$ just inside the wing leading edge using the square-root transformation (see Fig. 3b):

$$X_1+iY_1=\{[x-x_s(Z)]+i[\eta-\eta_s(Z)]\}^{1/2} \tag{20}$$

Finally, the bump representing the wing surface is sheared out according to

$$X=X_1, \quad Y=Y_1-Y_0(X,Z), \quad Z=Z \tag{21}$$

where $Y_0(X,Z)$ is the height of the mapped wing surface above the plane $Y=0$. Again, if the location of the singular line has been carefully chosen, $Y_0(X,Z)$ is a smooth function and the coordinate system is nearly orthogonal in planes of constant Z.

As in the case of the cylindrical/wind-tunnel transformation sequence, a Cartesian grid in the domain

$$-X_{\text{lim}} \le X \le X_{\text{lim}}, \quad 0 \le Y \le Y_{\text{lim}}, \quad 0 \le Z \le Z_{\text{lim}} \tag{22}$$

is mapped back to the physical domain to give the physical coordinates x,y,z of the mesh points after suitable stretchings in the X, Y, and Z directions to cluster the mesh lines in the vicinity of the body.

Two-dimensional interpolations are again necessary to determine the functions $Y_0(X,Z)$ and $Z_0(x,\eta)$ in terms of the input wing and fuselage geometry. Splines are used to interpolate the values of $Z_0(x,\eta)$ at each axial input station, with linear interpolation in the streamwise direction between input stations. The wing geometry is transformed according to Eqs. (18) and (19) and the modified wing sections are fitted with splines to provide section coordinates corresponding to the required mesh in the X direction. These data are linearly interpolated in the spanwise direction to give the wing coordinates at point in the computational mesh.

C. Boundary Conditions

Three types of boundary conditions must be specified to determine solutions for the potential flow past lifting wing-fuselage combinations. The no-flux condition must be enforced across any solid boundaries (such as the wing and fuselage surfaces); appropriate far-field boundary conditions must be specified at the necessarily finite limits of the computational domain; and appropriate jump conditions must be specified across the vortex sheet trailing behind the wing if it has lift.

The solid-surface boundary conditions are quite easy to enforce in boundary-conforming coordinate systems because the difference schemes are formulated in terms of the contravariant components of the velocity. The appropriate condition is that the out-of-plane component be zero. This is incorporated by reflection of the flux contributions for a given auxiliary cell in the fully conservative scheme, and by explicitly setting the velocity component to zero in the quasiconservative scheme.

A disadvantage of the finite-volume schemes is the need to truncate the usually infinite domains of aerodynamic interest to finite computational regions. This is in contrast to methods in which the equation can be transformed analytically with suitable stretching functions so that the difference mesh extends to infinity (see, e.g., Refs. 6, 9, and 10). In both of the analyses treated here, a reduced potential is introduced to describe the perturbations upon an otherwise uniform stream. This potential is set to zero on the upstream and lateral boundaries of the computational domain in both coordinate systems. The parabolic mapping shrinks the region of flow perturbed by the presence of the vortex sheet to a slit far downstream. The condition of zero-reduced potential is therefore also used at the downstream boundary in the Joukowsky/parabolic mesh system, except at the slit itself where the required discontinuity in potential is preserved. The streamwise perturbation velocity is set to zero at the downstream boundary in the cylindrical/wind-tunnel mesh system. This is consistent with the linear approximation that the pressure returns to its freestream value. A better approximation would be to solve the two-dimensional Laplace equation in the downstream boundary plane to determine the crossflow in this numerical approximation to the Trefftz plane.

The vortex sheet trailing downstream of a finite lifting wing is a contact discontinuity, across which the tangential components of velocity are discontinuous but the pressure is continuous. In reality, this surface is convected with the motion of the fluid, and rolls up on itself due to its self-induced velocities. In our analysis the convection and roll-up are ignored. Although this seems a gross approximation, it is thought that errors in the detailed shape of the vortex sheet will not have a major effect on the wing pressure distribution; in addition, a consistent model accounting for the roll-up of the sheet would add greatly to the difficulty of constructing a boundary-conforming coordinate system. The vortex filaments comprising the sheet are assumed to lie along the streamwise coordinates in a surface that leaves the wing trailing edge smoothly and lies nearly in the plane of the wing. Thus, a constant discontinuity in potential is continued downstream from the wing trailing edge in this surface, the value of the discontinuity being determined by the Kutta-Joukowksy condition that the pressures on the upper and lower surfaces match at the trailing edge. The values of the potential on the sheet are determined by requiring that the velocity normal to the linearized sheet be continuous. Incorporation of these constraints is simplified by the fact that the assumed vortex sheet location is also a boundary surface of the coordinate system for either mesh.

III. Results

A. Computational Considerations

Results calculated using three separate, but related, computer programs will be discussed in this section. These programs are based on various combinations of the above-described analyses, and will be referred to as follows.

FLO-25: Uses the quasiconservative difference scheme in the cylindrical/wind-tunnel coordinate system.

FLO-28: Uses the fully conservative difference scheme in the Joukowsky/parabolic coordinate system.

FLO-30: Uses the fully conservative difference scheme in the cylindrical/wind-tunnel coordinate system.

Note that FLO-25 and FLO-30 share the same mesh system for a given wing-fuselage geometry, while FLO-28 and FLO-30 use the same difference scheme.

All of the results to be presented here have been calculated on meshes containing $160 \times 24 \times 32$ cells in the X, Y, and Z directions, respectively. The convergence rate of a relaxation solution on this fine grid is painfully slow, so preliminary solutions are obtained on coarser grids and used as initial data for the fine-grid solutions. A sequence of three grids is generally used, each being obtained from the previous one by halving the grid spacing in each direction. Thus, each grid contains one-eighth the number of mesh cells of the succeeding grid, and the cost per iteration is almost an order of magnitude smaller. For the calculations presented here, 200 iterations were performed on each of the coarser grids, followed by 100 iterations of the finest grid. This procedure results in solutions of approximately the same level of convergence, measured by the reduction in maximum residual for each program, and the results can be meaningfully compared. On the finest grids, the lift may not be completely converged, but the expense of the calculation precludes a larger number of iterations. Recent experiments in two-dimensional calculations[11] show that a multigrid technique holds promise for achieving well-converged solutions at even less cost than the current runs. The present calculations require approximately 35 min of CPU time on the CDC 7600 and use 150 K (octal) of SCM and 260 K (octal) of LCM. The solution and coordinate arrays do not fit into even the LCM of this machine—they are stored on a disk file and are sequentially buffered in and out of core as needed for the relaxation process.

B. Sample Computations

Preliminary results of two of the methods have been previously presented[4,5] for a simple configuration consisting of the ONERA M-6 wing, low mounted on a cylinder whose axis was parallel to the wing plate. The wing geometry was identical to that tested by Monnerie and Charpin.[12] Results of calculations using FLO-25 and an early version of FLO-28 showed excellent agreement, but it was uncertain whether those minor discrepancies which did exist were due to differences in the mesh geometries or in the difference schemes themselves.

To further investigate the difference between the fully conservative and quasiconservative codes, a similar configuration was analyzed at a higher Mach number using the two difference schemes on the same coordinate grid. The configuration was made symmetric by moving the wing to the cylinder axis, and was analyzed at zero degrees angle of attack in order to eliminate the possibility of introducing compensating errors by minor differences in the way in which the Kutta-Joukowsky condition was applied. The configuration is illustrated in Fig. 4. Results were calculated for a freestream Mach number of 0.923 using both FLO-25 and FLO-30. Streamwise wing surface pressure distributions are shown for two span stations in Figs. 5a and 5b. The results are virtually indistinguishable, suggesting that the error introduced by the quasiconservative formulation is indeed small.

The next configuration to be analyzed consists of the same wing mounted at 3-deg incidence on a nonaxisymmetric fuselage. A perspective view of the wing and fuselage grids resulting from the cylindrical/wind-tunnel mapping for this configuration is shown in Fig. 6. The fuselage has a circular cross section, except in the vicinity of the wing-fuselage junction where nonaxisymmetric bulges have been added to simulate wing-root fairings. The configuration was analyzed at a freestream Mach number of 0.84 and zero degrees incidence with respect to the fuselage centerline. Results of calculations using FLO-28 and FLO-30 are presented in Figs. 7a and 7b. The first spanwise station at which results are shown corresponds to the wing-fuselage junction. Results of calculations on the two grid systems are in quite close

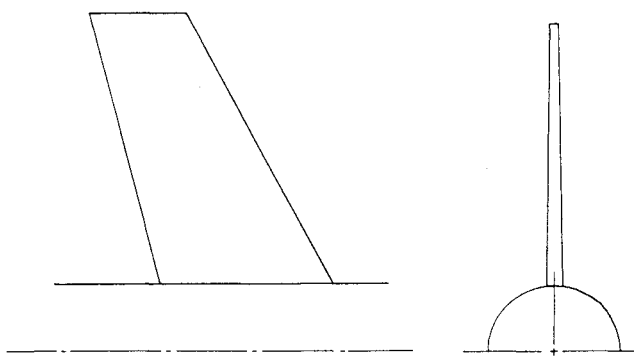

Fig. 4 Symmetric ONERA wing-cylinder configuration.

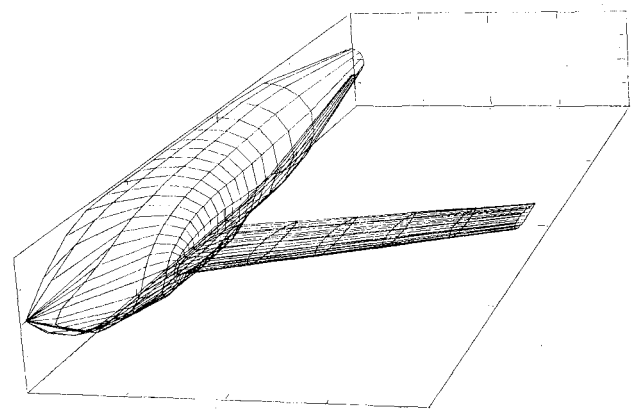

Fig. 6 Perspective view of wing and fuselage grids for ONERA wing mounted on nonaxisymmetric fuselage.

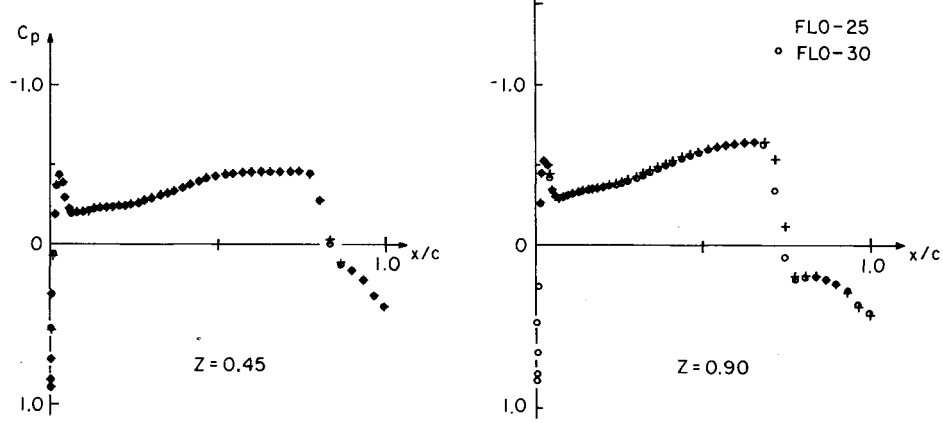

Fig. 5 Streamwise wing surface pressure distributions for symmetric ONERA configuration.

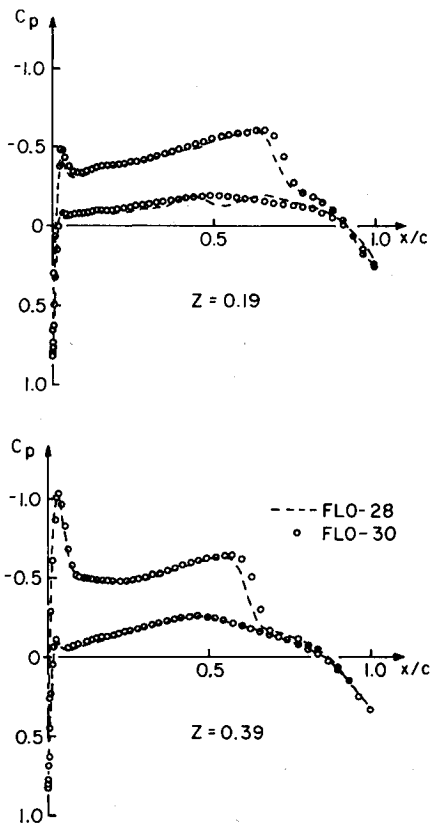

Fig. 7 Streamwise wing surface pressure distributions for ONERA wing mounted on nonaxisymmetric fuselage.

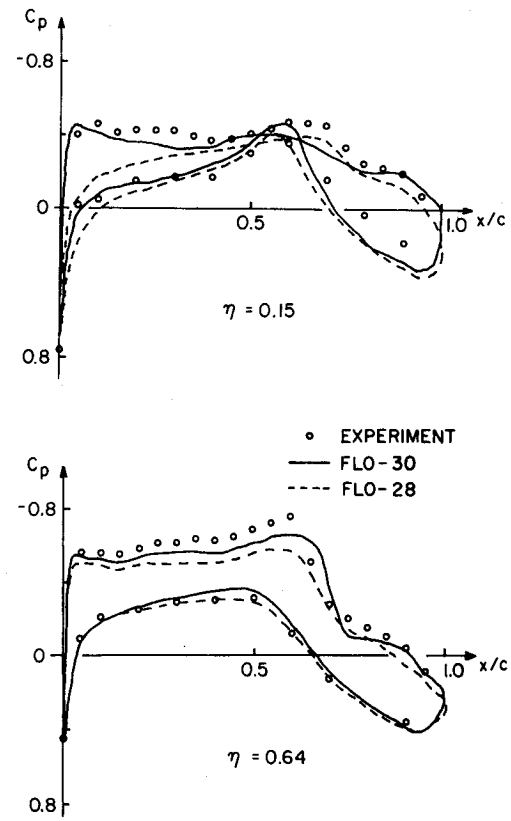

Fig. 9 Streamwise wing surface pressure distributions for transonic A-7 wing.

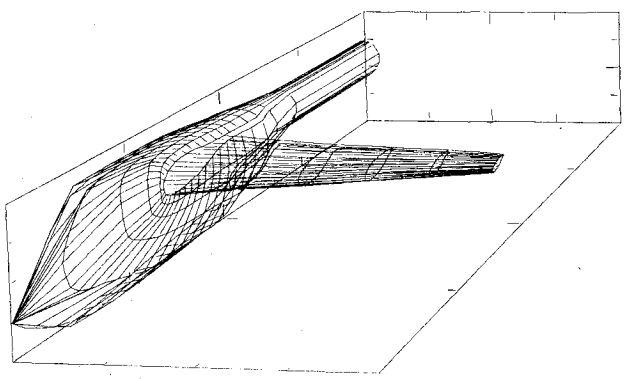

Fig. 8 Perspective view of wing and fuselage grids for A-7 with transonic wing.

agreement, except for small oscillations in the lower surface pressures calculated using FLO-28. These are caused by the fact that the Joukowsky/parabolic coordinate system is not completely boundary conforming, because the fuselage/symmetry-plane intersection is not a coordinate line. Therefore, the effective body in this mesh system has a number of small fins along the upper and lower fuselage/symmetry-plane intersections whose presence can have an effect upon the wing surface pressures. For this low-wing configuration, the effect is noticed primarily on the lower surface. These spurious fins become arbitrarily small as the mesh is continually refined, but even on the finest mesh used in these calculations the effect is apparent.

The last results to be presented are for a modern supercritical wing fuselage configuration which has been wind tunnel tested at the NASA Ames Research Center. A perspective view of the wing and fuselage grids is shown in Fig. 8. The configuration consists of a high-mounted swept wing of supercritical section mounted on a nonaxisymmetric fuselage, representative of the A-7 attack aircraft. Comparisons of calculated and experimentally determined wing surface pressure distributions at two span stations are shown in Fig. 9 for one of the conditions tested.[13] The freestream Mach number was 0.85 and the angle of attack of both the test and the calculation was 4.68 deg. The test Reynolds number was 3.8×10^6; no attempt was made to model viscous effects in the computation. Two calculations were performed using FLO-30 and FLO-28. The FLO-30 calculation was done for the complete wing-fuselage geometry pictured in Fig. 8 (including the wind-tunnel support sting); the FLO-28 calculation was performed for the wing alone, mounted on an infinite plane wall passing through the wing-fuselage junction. As can be seen, the pressure distributions are quite well-approximated by the results of FLO-30, the discrepancies easily falling within the range expected due to small angle-of-attack errors in the experiment or due to viscous effects. The underprediction of the lift by FLO-28 in the absence of the fuselage is an indication of the importance of the upwash due to the fuselage on the pressure distribution over the wing, especially at the inboard stations.

IV. Conclusions

Results of transonic potential flow calculations using the geometrically general finite-volume method have been presented for wing-fuselage combinations of varying complexity. Results of calculations on two different coordinate grids show that the solutions are relatively insensitive to details of the mesh geometry. The results of the quasiconservative and fully conservative difference schemes show remarkably good agreement in these calculations. However, there is no fundamental reason to believe that this will always be the case, except in the limit of weak shocks. Agreement with experimental data is quite good for geometries of current practical importance.

Appendix

A simple one-dimensional example serves to point out a shortcoming of the quasiconservative difference scheme and to indicate the limits within which reasonably accurate results might be obtained. Consider the one-dimensional potential equation

$$(1-M^{*2})\phi_{xx}=0 \tag{A1}$$

where $M^*=u/a^*$ is the dimensionless ratio of the fluid velocity $u=\phi_x$ to the sonic speed of sound a^*.

A quasiconservative difference approximation to Eq. (A1) can be written

$$(1-M_i^{*2})(\phi_{i+1}-2\phi_i+\phi_{i-1})+P_i-P_{i-1}=0 \tag{A2}$$

where the artificial viscosity terms are defined by

$$P_i=\mu_i(\phi_{i+1}-2\phi_i+\phi_{i-1}) \tag{A3}$$

with the switching function μ_i defined as

$$\mu_i=\max(M_i^{*2}-1,0) \tag{A4}$$

The velocities are determined by the central-difference formulas

$$M_i^*=(\phi_{i+1}-\phi_{i-1})/2\Delta x \tag{A5}$$

This scheme reproduces the Murman parabolic and shock-point operators when $\mu_{i-1}\leq 0\leq\mu_i$ and $\mu_i\leq 0\leq\mu_{i-1}$, respectively. The jump relations are determined by the form of the shock-point operator:

$$(1-M_i^{*2})(\phi_{i+1}-2\phi_i+\phi_{i-1})$$
$$+(1-M_{i-1}^{*2})(\phi_i-2\phi_{i-1}+\phi_{i-2})=0 \tag{A6}$$

The solution in the vicinity of a shock consists of a piecewise linear representation of ϕ as a function of x, with the shock corresponding to a discontinuity in ϕ_x. Let the shock be located a fraction α of the way between the $(i-1)$st and the ith mesh points, and let M_1^* and M_2^* represent the dimensionless velocities of the exact solution upstream and downstream of the shock, respectively. The central-difference velocities needed in Eq. (A6) are then seen to be

$$M_i^* = ((2-\alpha)M_2^*+\alpha M_1^*)/2$$

$$M_{i-1}^* = ((1-\alpha)M_2^*+(1+\alpha)M_1^*)/2 \tag{A7}$$

In terms of the velocities M_1^* and M_2^*, Eq. (A6) can thus be written

$$M_2^*=\frac{(-1+\alpha-\alpha^2)M_1^*+2[\alpha(\alpha-1)M_1^{*2}+(1+\alpha-\alpha^2)]^{1/2}}{(1+\alpha-\alpha^2)} \tag{A8}$$

This is the normal shock relation for the quasiconservative scheme and shows the dependence of the solution upon the parameter α. If the shock is located at a mesh point, $\alpha=0$, and

$$M_2^*=2-M_1^* \tag{A9}$$

The minimum value of M_2^* can be shown to result when the shock is midway between two mesh points, i.e., when $\alpha=\frac{1}{2}$. In this case,

$$M_2^*=-0.6M_1^*+0.8(5-M_1^{*2})^{1/2} \tag{A10}$$

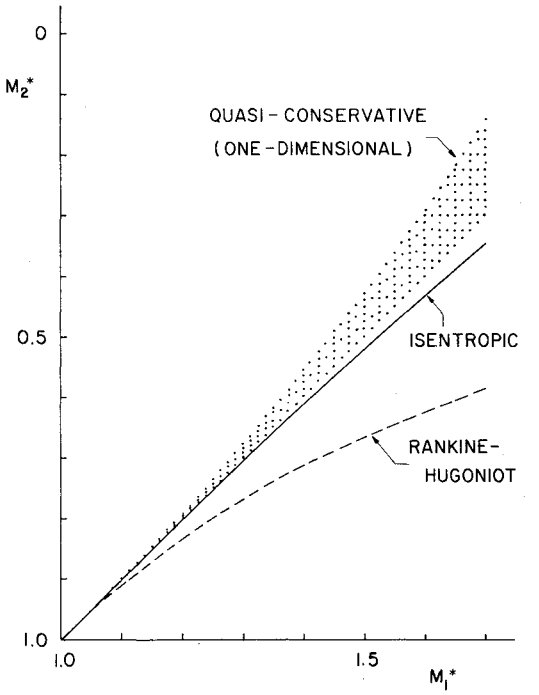

Fig. A1 Shock relations for quasiconservative and fully conservative (isentropic) schemes.

These results are pictured in Fig. A1. The shaded region represents the range of possible values of M_2^* as α varies from 0 to ½; the lower boundary of the shaded region represents the curve for $\alpha=0$, while the upper boundary is that for $\alpha=\frac{1}{2}$. The range of possible downstream states is quite large for M_1^* greater than about 1.3. This result carries the implication that solutions using such a difference scheme are dependent upon the location of the shock waves within the mesh cells. In particular, such solutions cannot be expected to converge in the limit of small mesh spacing, except in the rather special case when all shocks are located exactly at mesh points.

The remarkable agreement between the calculated results of the quasiconservative and fully conservative schemes is almost certainly due to the fact that the shock relations of both schemes agree quite well in the limiting case of weak shocks. As can be seen, the range of possible solutions for different values of α becomes quite small for M_1^* less than about 1.2; for these values, the result also agrees well with that for a mass-conserving isentropic shock also shown in the figure. For comparison, the jump relation for a Rankine-Hugoniot normal shock is also plotted. Of particular interest is the fact that the discrepancy due to the quasiconservative formulation is small when the isentropic approximation is appropriate.

In summary, this one-dimensional argument provides a theoretical basis for the good agreement which is observed between results of calculations using quasiconservative and fully conservative difference schemes for the potential equation when the shocks are weak. Due to the dependence of the jump relations on the fractional spacing of the shock within the mesh cell, however, solutions using the quasiconservative scheme cannot, in general, be expected to converge to a unique solution as the mesh is continually refined.

Acknowledgments

This work was supported in part by the Office of Naval Research under Contracts N00014-77-C-0033 and N00014-78-C-0079, and by the NASA Ames Research Center under Contract NAS-9913.

References

[1] Caughey, D. A. and Jameson, A., "Calculation of Transonic Potential Flowfields about Complex, Three-Dimensional Configurations," *Transonic Flow Problems in Turbomachinery*, edited by T. C. Adamson and M. F. Platzer, Hemisphere Publishing Corp., Washington, D.C., 1977, pp. 274-291.

[2] Carlson, L. A., "Transonic Airfoil Analysis and Design using Cartesian Coordinates," *Proceedings of AIAA 2nd Computational Fluid Dynamics Conference*, Hartford, Conn., June 1975, pp. 175-183.

[3] Reyhner, T. A., "Cartesian Mesh Solution for Axisymmetric Transonic Potential Flow around Inlets," *AIAA Journal*, Vol. 15, May 1977, pp. 624-631.

[4] Jameson, A. and Caughey, D. A., "A Finite-Volume Method for Transonic Potential Flow Calculations," *Proceedings of AIAA 3rd Computational Fluid Dynamics Conference*, Albuquerque, N. Mex., June 1977, pp. 35-54.

[5] Caughey, D. A. and Jameson, A., "Numerical Calculation of Transonic Potential Flow about Wing-Body Combinations," *AIAA Journal*, Vol. 17, Feb. 1979, pp. 175-181.

[6] Jameson, A., "Iterative Solution of Transonic Flows over Airfoils and Wings Including Flows at Mach 1," *Communications on Pure and Applied Mathematics*, Vol. 27, 1974, pp. 283-309.

[7] Garabedian, P. R., "Estimation of the Relaxation Factor for Small Mesh Size," *Mathematical Tables and Aids to Computation*, Vol. 10, 1956, pp. 183-185.

[8] Caughey, D. A., "A Systematic Procedure for Generating Useful Conformal Mappings," *International Journal for Numerical Methods in Engineering*, Vol. 12, 1978, pp. 1651-1657.

[9] Jameson, A. and Caughey, D. A., "Numerical Calculation of the Transonic Flow Past a Swept Wing," New York University ERDA Rept. C00-3077-140, June 1977.

[10] Caughey, D. A. and Jameson, A., "Accelerated Iterative Calculation of Transonic Nacelle Flowfields," *AIAA Journal*, Vol. 15, Oct. 1977, pp. 1474-1480.

[11] Jameson, A., "A Multi-Grid Scheme for Transonic Potential Calculations on Arbitrary Grids," *Proceedings of AIAA 4th Computational Fluid Dynamics Conference*, Williamsburg, Va., July 1979, pp. 122-146.

[12] Monnerie, B. and Charpin, F., "Essais de buffeting d'une aile en fleche en transsonique," *10e Colloque d'Aerodynamique Applique*, Lille, France, Nov. 1973.

[13] Hicks, R. M., NASA Ames Research Center, private communication, Oct. 1979.